Chondroitin sulfate is required for the organ development and maintenance in *Drosophila*

A Thesis
SUBMITTED TO THE FACULTY OF THE
UNIVERSITY OF MINNESOTA
BY

Woo Seuk Koh

IN PARTIAL FULFILLMENT OF THE
REQUIREMENTS
FOR THE DEGREE OF
MASTER OF SCIENCE

Hiroshi Nakato

June, 2022

Acknowledgements

We thank Dr. Stéphane Noselli and the laboratory of Véronique Van De Bor for the donation of anti-Vkg primary antibody.

This work was supported by the National Institutes of Health (R35 GM131688) to H.N. WSK was supported by grant T32GM140936 from the National Institutes of Health.

Abstract

Heparan sulfate (HS) and chondroitin sulfate (CS) are evolutionary conserved glycosaminoglycans that are found in most animal species, including a genetically tractable model organism *Drosophila*. In contrast to extensive in vivo studies elucidating co-receptor functions of *Drosophila* HSPGs, only a limited number of studies have been conducted for those of CSPGs. This is partly due to the lack of in vivo model systems to systematically study the functions of *Drosophila* CSPGs in development. To investigate the global function of CS in development, we have generated mutants for *Chondroitin synthase* (*Chsy*), which encodes the *Drosophila* homologue of chondroitin synthase 1 (ChSy-1), via CRISPR-Cas9 mutagenesis. Our characterizations of the *Chsy* mutants indicated that a fraction of the mutants survive to adult stage, which allowed us to analyze the morphology of the adult organs. *Chsy* mutants exhibited a gradual disruption of the basement membrane (BM) and a subsequent degradation of the gross organ structure as mutant animals aged. The age-dependent decay of the ovary structure observed in the *Chsy* mutants suggests that normal CS function is required for the maintenance of the structural integrity of the ECM and gross organ architecture.

Table of Contents

List of Tables

List of Figures

Introduction

The *Drosophila* ovary is an excellent model system to study organ development and maintenance (Fig.1). The ovary is the largest organ in the female abdomen (Fig.1A) and is composed of ovarioles, which are strings of progressively developing egg chambers through the process of oogenesis (Fig.1B). Germline stem cells (GSCs) are located at the anterior end of the ovary in a structure known as the germarium (Fig.1C). Each germarium has two or three GSCs that are in direct contact with the specific somatic cells known as cap cells.

The ovary is also known as a powerful model to study *in vivo* functions of the basement membrane (BM) (Fig.1B), which is a special set of ECM polymers basally underlying the epithelia or other tissues and imparts significant contributions to the organ development as well as its shape and size maintenance (Ramos-Lewis and Page-McCaw, 2019). For example, core components of the BM such as collagen IV (ColIV) exerts influence on the proper organ development, maintenance, and organization (Van De Bor *et al*., 2021). Another core component called Perlecan provides the structural foundation for the BM (Diaz-Torres *et al.*, 2021). Moreover, stiffness of the BM in the ovary influences shaping of the organ (Haigo and Bilder, 2011).

The BM can affect organ development via different mechanisms and in addition to its mechanical functions, BM participates in morphogen signaling, in which it contributes to various developmental processes including cell differentiation, proliferation, survival, polarization, and migration via exerting influence, directly and indirectly, on signaling (Daley and Yamada, 2013; Howard *et al*., 2019; Morrissey and Sherwood, 2015; Ramos-Lewis and Page-McCaw, 2019; Yurchenco, 2011). For

example, BM affects signaling to its contacting cells by binding or sequestering specific signaling ligands (Isabella *et al.*, 2015, Ma *et al.*, 2017).

Proteoglycans (PGs) are a special class of carbohydrate-modified proteins that have glycosaminoglycan (GAG) chains covalently attached to the core protein (Varki *et al*., 1999). Heparan sulfate (HS) and chondroitin sulfate (CS) are the most evolutionarily conserved GAGs that are found in most animal species, including C. elegans, Drosophila and vertebrates. HSPGs are well established as co-receptors for growth factor signaling, regulating distribution and reception of secreted signaling proteins (Lindahl, 2009; Esko and Selleck, 2002; Kirkpatrick and Selleck, 2007; Nakato and Li, 2016; Xu and Esko, 2014). Genetic studies using the Drosophila model have helped establish that roles of HSPGs in morphogen signaling (Nakato and Li, 2016) and also in stem cell control (Bowden and Nakato, 2021). In Drosophila, HS-dependent secreted factors include FGFs, Decapentaplegic (Dpp; a *Drosophila* BMP), Wingless (Wg; a *Drosophila* Wnt), Hedgehog (Hh) and Unpaired (Upd; a ligand of the JAK/STAT pathway) (Nakato, 2016). For example, Dally, a Drosophila HSPG of the glypican-type, acts as a Dpp co-receptor to regulate its signaling and gradient formation in the developing wing (Fujise *et al.*, 2003; Belenkaya *et al.*, 2004; Akiyama *et al.*, 2008). In the ovary, Dally controls the maintenance of germline stem cells (GSCs) and stalk formation (Hayashi *et al*., 2009; Guo and Wang, 2009; Hayashi *et al.*, 2012).

During the biosynthesis of HS, the chain is polymerized by Ext proteins that function as HS co-polymerases. *tout-velu* (*ttv*) encodes the *Drosophila* homologue of Ext1, a key component of the co-polymerase complex. *ttv* mutants fail to synthesize HS (Toyoda *et al*., 2000). The first step of the HS modification, deacetylation and sulfation of the GlcNAc residue, is catalyzed by HS *N*-deacetylase/*N*-sulfotransferases (Ndsts)

(Ballaiche *et al*., 1998). Since this step is prerequisite to the following modification reactions, the lack of Ndsts results in the synthesis of non-sulfated heparan sulfate (Toyoda *et al*., 2000). Sulfateless (Sfl) is the only *Drosophila* homologue of Ndsts, and *sfl* mutation abolishes most, if not all, biological functions of HS (Lin *et al*., 1999). Both *ttv* and *sfl* mutants have been extensively used as HS-deficient animal model systems to define the *in vivo* functions of HS in various biological contexts (Ballaiche *et al*., 1998; Toyoda *et al*., 2000; Reynolds-Peterson *et al*., 2017).

In contrast to extensive in vivo studies elucidating co-receptor functions of HSPGs, only a limited number of studies have been conducted for those of *Drosophila* CSPGs. This is partly because in vivo model systems to systematically study the functions of CSPGs in development are lacking. We recently identified a novel Drosophila CSPG, Windpipe (Wdp) (Takemura *et al.*, 2020). Wdp is a single-pass transmembrane protein containing three GAG chains and leucine-rich repeat (LRR) motifs, and is a novel regulator of the Hedgehog signaling pathway (Takemura *et al*., 2020). However, Wdp is one of very few CSPG molecules that have been identified and investigated in *Drosophila*, while more than 25 are known in *C. elegans* (Noborn *et al*., 2018). This suggests that many *Drosophila* CSPGs remain to be discovered. Since CSPG core proteins are not well-conserved between species (Olson *et al.*, 2006), the identification of CSPGs cannot rely on the sequence homology to mammalian counterparts. It is therefore important to elucidate the global function of CS using the mutant animals that lack a component of the CS biosynthetic pathway.

In mammals, the polymerization of CS is achieved by enzyme complexes composed of multiple proteins that function redundantly (Mikami and Kitagawa, 2013). Chondroitin synthase 1 (ChSy-1) is the key enzyme of these polymerase complexes. Due

to this redundancy, ChSy-1 knockout mice are viable although the CS production is reduced (Wilson *et al*., 2012). In humans, loss of ChSy-1 causes temtamy preaxial brachydactyly syndrome (Li *et al*., 2010; Tian *et al*., 2010). In *C. elegans*, where there is less redundancy in the CS polymerases, this gene is known as *squashed valva 5* (*sqv5*) because its loss of function disrupts the invagination of the vulval epithelium (Herman and Horvitz, 1999). In addition, the mutants show a defect in the progression of cytokinesis in early embryos, abnormal distal tip cell migration, and reduced levels of chondroitin (Mizuguchi *et al.*, 2003; Suzuki *et al*., 2006). Although the *Drosophila* genome has a few genes that show homology to the human CS polymerases, it is unknown how the CS chains are polymerized in this model organism.

In this study, we investigate the global function of CS using the mutant *Drosophila* model that lacks the functional ability of *chondroitin synthase* (*Chsy*), which is a component of the CS biosynthetic pathway that encodes the homologue of mammalian *ChSy-1*. Our biochemical analyses of isolated CS from the mutants show that the *Chsy* mutations significantly impair the 4-*O* sulfation of GalNAc residues. Further, we characterize five distinct morphological defects observed in the *Chsy* mutant ovarioles and other developmental aberrations caused by the altered CS function in an age-dependent manner. Importantly, our results suggest a synergistic effect of the observed defects that eventually leads to a subsequent degradation of the gross organ architecture. Hence, our findings indicate that possible interconnections or genetic interactions exist behind the aberrant phenotypes observed. Using the *Drosophila* molecular genetic tools as our model, our study reveals that normal CS biosynthesis is necessary for the proper development and maintenance of gross organ architecture, as well as the structural integrity of the ECM.

Results

Generation of *Chsy* mutant: A novel CS-Deficient animal model

To investigate the global function of CS in development, we have generated mutants for *Chondroitin synthase* (*Chsy*) using CRISPR-Cas9 mutagenesis. *Chsy* encodes the *Drosophila* homologue of human chondroitin synthase 1 (ChSy-1). Due to the presence of another gene (*alkaline phosphatase 11*) within the third intron of *Chsy*, we have designed two different deletions ($Chsy^1$ and $Chsy^2$), one on each side (Fig.2). Both mutations remove a large portion of the coding sequence but do not affect the intronic alkaline phosphatase 11 gene. The $Chsy^2$ allele removes the enzyme catalytic site (arrow, Fig.2), and is thus considered as a null allele.

As a first step to characterize the *Chsy* mutant alleles, we conducted a lethality analysis. $Chsy^2$ allele revealed significantly higher lethality than $Chsy^1$ (Fig.3, Table 1). This result suggests a possibility that $Chsy^1$ allele may not be a null. We will discuss this later.

Moreover, in contrast to the wild-type animals, adult survivors of both *Chsy* alleles showed a folded wing phenotype (Fig.4A-B). A typical affected wing had its distal region remaining folded, while the proximal part was partially expanded (Fig.4B). And mutants of both alleles showed high penetrance of approximately 75% on average (Fig.4C, Table 2). Interestingly, wing patterning, which can be observed in unfolded wings, did not show any gross defect. This indicates that *Chsy* mutants show a defect in the wing maturation process, the last step of wing development (Kiger *et al.*, 2001; Kiger *et al.*, 2007; Bilousov *et al.*, 2012).

CS polymerization is disrupted in *Chsy* mutants

To determine the molecular basis for the *Chsy* mutant phenotypes, we examined the structure of CS isolated from the mutants by disaccharide analysis (Fig.5). Briefly, CS was purified from wild-type and *Chsy* mutant adult flies, and completely digested into disaccharides by condroitinase ABC. The resultant disaccharide species, ΔDi-0S and ΔDi-4S, were separated and quantified by reversed-phase ion-pair chromatography with post-column detection system (Toyoda *et al.*, 2000; Kamimura *et al.*, 2006; Kleinschmit *et al.*, 2010; Dejima *et al.*, 2013; Nakato *et al.*, 2019). We found that CS is completely undetectable in $Chsy^2$. On the other hand, we detected residual ΔDi-0S disaccharide but not ΔDi-4S in $Chsy^1$.

Consistent with the lethality assay data, this observation supports the idea that $Chsy^2$ is a null allele but $Chsy^1$ is not. We found that there is a methionine residue in frame in the fourth exon (asterisk, Fig.2). Therefore, a mRNA from the $Chsy^1$ locus can still encode a truncated protein with the enzyme catalytic site, which may have a residual activity. These results suggest that $Chsy^1$ is a strong hypomorphic allele. Hereafter, we focused on $Chsy^2$ in the subsequent analyses. The *Chsy* mutant alleles represent the first CS-deficient animal model in *Drosophila*.

***Chsy* mutants display developmental delay and defects in reproductive quality/ability**

Throughout our study, we had noticed slow development in the *Chsy* mutants in comparison to the wild-type animals. Additionally, a previous study indicated that improper ColIV synthesis induces various aberrant phenotypes in the organ architecture that ultimately engenders compromised female fertility (Van De Bor *et al*., 2021).

Stemming from these observations, we analyzed the developmental time duration and reproductive ability of *Chsy* mutants. We observed that *Chsy* mutants show drastic delay in development compared to wild-type animals and undermined reproductive ability as indicated by a significant reduction in the number of eggs laid (Fig.6A-B, Table 3A-B). Moreover, proportion of eggs that hatched was significantly lower for *Chsy* mutants than for wild-type and its severity became prominently higher with age (Fig.6C, Table 3C). These observations suggested that the quality of eggs laid by the mutants is abysmal and the probability of female sterility increases over time.

Chsy mutants show a defect in organ shape maintenance and oogenesis

One obvious abnormality in *Chsy* mutants is their high levels of infertility. We noticed that *Chsy* female adults lay few eggs only at young stages, suggesting that CS plays a role in oogenesis. As a first step to study the function of *Chsy* during oogenesis, we analyzed the gross ovary morphology of *Chsy* mutants at different ages after eclosion (Fig.7). The ovarioles were stained with anti-FasIII (for follicle cells) and anti-Vasa (for germ cells) antibodies.

In wild-type, ovaries of the old (day-21 after eclosion) animals retained normal organ structures, indicating that no major defects in the ovary morphology or oogenesis emerged with age (Fig.7A). We observed no significant abnormalities in the ovary morphology from young (day-3 after eclosion) mutant animals. In contrast, the ovariole morphology from aged *Chsy* mutants (day-21) was massively altered with decreased size (Arrows, Fig.7B). In these ovarioles, individual egg chambers show abnormal shape and lack a spatiotemporally ordered alignment during oogenesis (Arrowheads, Fig.7B).

We examined further details of morphological defects of *Chsy* mutant ovaries. In wild-type, oogenesis progresses with a proper organization of the growing egg chambers of 14 stages, each consisting of a germline cyst enclosed by a follicular epithelium, in a spatiotemporal order (Spradling, 1993; Antel *et al.*, BioRxiv). We confirmed that wild-type ovarioles showed intact structural integrity and proper progression of oogenesis at young, mid-, and old ages, indicating the maintenance of normal organ development throughout the progression of age (Fig.7C). In contrast, however, *Chsy* mutants displayed a gradual deterioration in ovariole structural integrity with various morphological defects (Fig.7D). Remarkably, we observed five distinctive phenotypic categories as described below (Fig.8A-E).

First, *Chsy* mutant ovarioles demonstrated an abnormality in the conformation of developing egg chambers, yielding a 'compressed' egg chamber phenotype (Arrows, Fig.8A). In wild-type, early stage egg chambers (typically Stage 4 and earlier) are spherical in shape, which then lengthen along the anterior-posterior (AP) axes into the oval shape as they mature into later stages (Cetera *et al*., 2014). In contrast, *Chsy* mutant ovarioles were characterized by the premature onset of asymmetrical and flattened ellipsoid-shaped egg chamber elongation either at the AP axis or perpendicularly to the AP axis (Fig.8A). Further, even the egg chambers at the later stages of oogenesis sporadically manifested similar morphogenesis abnormality. Possible rationales for the premature and irregularly-shaped egg chamber elongation defect may be due to aberrations in the rotation of developing egg chambers and/or the contractions of oscillating basal actomyosin (He *et al*., 2010; Haigo and Bilder, 2011; Gates, 2012). For example, it was previously indicated that collagen type IV (ColIV) is necessary to sustain the appropriate orientation of the basal actin filaments (Yasothornsrikul *et al*, 1997;

Haigo and Bilder, 2011; Gates, 2012). It was also shown that defects in egg chamber rotation and elongation became apparent with the distorted orientation of *viking* (*vkg*), which encodes the α2 chain of *Drosophila* ColIV (Yasothornsrikul *et al.*, 1997; Haigo and Bilder, 2011; Gates, 2012). Hence, it is possible that the normal polarization of protein networks which regulate the egg chamber rotation and/or morphogenesis is disturbed in the *Chsy* mutants. Such defect during oogenesis can eventually induce the compressed egg chamber phenotype.

Second, we observed that a germline cyst is covered by two or more epithelial layers, instead of a normal single layer, in *Chsy* mutant egg chambers (Arrow, Fig.8B). In some cases, the epithelial cell clusters are intruded into the germline cyst (Arrowheads, Fig.8B). These phenotypes were previously reported in mutants for genes that control cell polarity, morphogenesis, cell proliferation, adherens junction (AJ) organization, and vesicle transport (Builder *et al*., 2000; Lu and Bilder, 2005; Fernández-Miñán *et al*., 2007; Georgiou *et al*., 2008; Harris and Tepass, 2008; Leibfried *et al*., 2008; Morrison *et al*., 2008; Franz and Riechmann, 2010; Berns *et al*., 2014). For example, upregulation of genes such as the polarity regulator *par-6* and the actin cross-linker *α-Spectrin* manifested prominent cases of epithelial multilayering in the *Drosophila* ovarioles (Berns *et al*., 2014). Further, it was previously reported that knockdown of the tumor repressor gene *lgl* triggered overproliferation and intrusion of epithelial cells into germline cysts (Builder *et al*., 2000; Berns *et al*., 2014).

We also observed that there are gaps of follicular epithelium where the cyst is not covered by epithelial cells (Arrow, Fig.8C). Potential explanations for this 'epithelial rupture' phenotype include a defect in cell adhesion or actin cytoskeleton, resulting in the compromised epithelial integrity (Wang and Riechmann, 2007; Berns *et al*., 2014;

Lovegrove *et al.*, 2019). For example, it was shown that knockdown of genes like *Kugelei* or *kon-tiki*, which regulate cell adhesion and cytoskeletal organization, triggered ruptures in epithelia (Schnorrer *et al*., 2007; Berns *et al*., 2014). Further, it was indicated that knockdown of genes that directly or indirectly affect progression of epithelial cell cycle such as *fascetto* resulted in the reduction of epithelial cells and damaged epithelia (Berns *et al*., 2014).

Fourth, a 'compound egg chamber' phenotype was observed in the ovarioles of *Chsy* mutants (Fig.8D). This phenotype is characterized by the impaired cyst separation, in which one epithelial monolayer encloses two or more germline cysts. It was reported that genes associated with the causation of a compound egg chamber phenotype frequently led to epithelial ruptures, or compound follicles co-occurred with incomplete cyst encapsulation by follicle cells (Hongay and Orr-Weaver, 2011; Berns *et al*., 2014[14], Chanet and Huynh, 2020). Likewise, it was shown that a reduction in the follicle cell number or disruption in the ovariole epithelium also induced compound egg chamber phenotype (Bäumer *et al*., 2012; Berns *et al*., 2014).

Furthermore, *Chsy* mutants exhibit 'fused egg chambers' (Fig.8E). The affected ovarioles, while each germline cyst was properly enclosed by an epithelial monolayer, showed a failure in the separation of individual egg chambers. This may be caused by the defect in the stalk formation. A previous study showed that 65% of the genes causing fused egg chambers also induced the compound phenotype (Berns *et al*., 2014). We have previously shown that the loss of HS biosynthetic genes (e.g. sfl) in follicle cells disrupts Upd signaling, leading to the lack of stalks and fused egg chambers (Hayashi, 2012).

Importantly, the penetrance for all these phenotypes increases as animals age (Fig.8A-E). Thus, in *Chsy* mutants, the ovary formation occurs relatively normally, but

the mutants fail to maintain the organ shape during aging: they show a gradual decay of the gross organ structure in an age-dependent manner. At day-21 after eclosion, a severe failure in the maintenance of structural integrity and abnormal oogenesis became evident in the ovarioles of *Chsy* mutants, in which all aberrant ovarioles observed were marked by a reduction in the number of at least one or more mid-stage egg chambers (Fig.8A-E).

Together with the previous studies, our observations strongly suggest that *Chsy* functions as a key regulator in the organ development by playing an influential role in many genetic pathways involved.

Apicobasal polarity of follicle cell epithelia and their adhesion to the germline are disrupted in *Chsy* mutants

Possible rationales for the abnormal epithelial development observed in *Chsy* mutants include impairments in the AJ organization and cell polarity. To test this idea, we analyzed AJ structures in the mutant ovarioles. During egg chamber development, follicle cells (FCs) are polarized in a way that the apical side contacts the germ cells (Fig. 9). This attachment requires cadherin-based adhesion and AJ structures (Antel *et al.*, BioRxiv). In wild-type, Armadillo (Arm), the Drosophila b-catenin, is properly localized near the boundary of FCs and germline cysts, showing normal polarity of FCs and appropriate AJ organization (Fig.9A-B). In contrast, AJ is frequently mislocalized in FCs of the *Chsy* mutant egg chambers (Fig.9C-D). The AJ is relocalized from the apical to the basal/lateral side, suggesting that the apicobasal polarity of FCs is disrupted (Arrowheads, Fig.9D). Remarkably, Arm was sometimes localized between the nurse cells inside the germline cysts instead of the FC-germline boundaries in the mutants (Arrow, Fig.9D). A previous report showed that ingression of epithelial cells into the

cysts caused abnormal localization of AJ structures (Builder *et al*., 2000; Berns *et al*., 2014; Chanet and Huynh, 2020). Similar to other phenotypes, the penetrance of this abnormality increases during aging (Fig.9D).

Chsy mutants show defects in the proper specification of stalk cell fate

The fused egg chambers phenotype of *Chsy* mutants suggested that the proper specification of stalk cells is impaired in these mutants. It has been shown that the absence of proper stalk formation triggers fused egg chambers during oogenesis (Berns *et al*., 2014; Antel *et al.*, BioRxiv). Anti-Lamin C antibody, a stalk cell marker, of wild-type ovarioles revealed normal stalk formations between individual egg chambers (Fig.10A-B). Similarly, a majority (>75%) of the young *Chsy* mutant ovarioles reflected proper specification of the stalk cells (Fig.10C,E). However, 85% of aged (day-21) *Chsy* mutant ovarioles showed a defect in the proper specification of stalks that resulted in the complete abolishment of one or more stalks (Arrow in Fig.10D, E). Consistent with previous reports, this defect was often accompanied by fused or compound egg chambers (Berns *et al*., 2014; Antel *et al.*, BioRxiv).

Interestingly, *Chsy* mutants also exhibited a misplacement of stalk cells. In these ovarioles, Lamin C-positive stalk cells appeared at random locations in between as well as around the egg chambers, and failed to assemble in the normal 'beads-on-a-string' configuration (Arrowhead in Fig.10D). This phenotype was observed in 20% of the aged mutant ovarioles (Fig.10F).

BM becomes morphologically disorganized in _Chsy_ mutants

The basement membrane (BM) is a thin, specialized ECM basally underlying epithelia, and directly contributes to various developmental processes, including cell differentiation, proliferation, survival, polarization, and migration (Yurchenco, 2011; Daley and Yamada, 2013; Morrissey and Sherwood, 2015; Ramos-Lewis and Page-McCaw, 2019). ColIV, a main component of the BM, is required for normal stalk morphogenesis as well as structural integrity overall (Van De Bor et al., 2021). ColIV fibrils also play important roles in conveying mechanical constraint to promote proper shaping of egg chambers (Haigo and Bilder, 2011; Bilder and Haigo, 2012; Daley and Yamada, 2013; Isabella and Horne-Badovinac, 2016; Crest *et al.*, 2017).

Since *Chsy* mutants showed similar abnormalities in the specification of stalk cell fate, we asked if *Chsy* mutations affect the BM structure. *Chsy* mutant ovarioles were stained with antibody against Viking (Vkg), the α2 chain of *Drosophila* ColIV (Fig.11; Van De Bor *et al*., 2021). In the wild-type ovarioles, normal formation of the BM was observed at all ages. Likewise, young *Chsy* mutant ovarioles did not show any aberrant BM structures (Fig.11A-C). In contrast, as *Chsy* mutant animals aged, the BM became morphologically disorganized, leading to alterations in the gross architecture of ovarioles (Arrow, Fig.11D). Moreover, affected BMs in the *Chsy* mutant ovarioles were also characterized by the presence of numerous interstices within the layers, showing a 'chain-like' morphology (Arrowheads, Fig.11D). As indicated by several previous studies, it is possible that *Chsy* mutants may have altered mechanical properties of the BM, causing abnormality in the shaping of developing ovarioles and defects in oogenesis (Haigo and Bilder, 2011; Bilder and Haigo, 2012; Daley and Yamada, 2013; Isabella and Horne-Badovinac, 2016; Crest *et al*., 2017; Van De Bor *et al*., 2021). Nonetheless, these results suggested that the initial assembly of the organ can occur in the absence of *Chsy* but the

normal CS function is required for the maintenance of the structural integrity of the BM and organ shape by adult stage-specific role of *Chsy*.

Discussion

A novel function of CS in the organ development and maintenance

In *Drosophila*, many factors can contribute to and must be properly assembled for the normal development and maintenance of organs. One example is intact co-receptor functions for morphogen signaling, such as previously established roles of HSPGs in growth factor morphogen signaling (Nakato and Li, 2016) and in stem cell control (Bowden and Nakato, 2021). In addition, recent studies have shown that the BM directly affects the development of organs, maintaining the proper organ shape/size (Ramos-Lewis and Page-McCaw, 2019). However, it has been a major challenge to define the mechanism by which the BM functions in organ development due to the complexity in which its mechanical properties (e.g. stiffness, elasticity) are dictated by its composition, geometry and cross-linking, affecting the behavior of the contacting cells. Nonetheless, the BM can affect organ development via different mechanisms: First, the BM affects signaling to contacting cells by binding or sequestering specific signaling ligands (Isabella *et al.*, 2015, Ma *et al.*, 2017). Second, the BM provides physical support for cells and affects the development of associated tissues through mechanotransduction (Isabella *et al.*, 2015, Ma *et al.*, 2017).

However, in contrast to numerous findings on the roles of HSPGs, not much have been established for those of CSPGs. This is mainly due to a difficulty in the identification of CSPGs since CSPG core proteins are not well-conserved between species (Olson et al., 2006). Therefore, we have investigated the global function of CS using the mutant animals that lack a component of the CS biosynthetic pathway. In this report, we introduce the novel functions of CS and have characterized the mechanisms by

which CS regulates organ development, its maintenance, and the BM morphology. We propose that the initial assembly of the organ can occur in the absence of *Chsy* but normal CS function is required for the maintenance of the structural integrity of the ECM and gross organ architecture.

Characterization of *Chsy* mutant phenotypes

First, our results from the biochemical analyses of CS demonstrate that the 4-*O* sulfation of GalNAc residues is notably undermined in the *Chsy* mutant animals without impacting the total amount of CS production. On top of that, our preliminary probes evince that *Chsy* mutation instigates anomalies in wing maturation and qualitative abilities of reproduction, as well as a delay in development.

Accompanied by our findings from the incipient screenings, we found that *Chsy* mutants show a combination of very unique age-dependent phenotypes leading to abnormal oogenesis and a severe failure in the maintenance of organ structural integrity. As animals age, *Chsy* mutant ovarioles display increasing cases of compressed egg chambers, multi-layered epithelia, epithelial rupture, compound egg chambers, and/or fused egg chambers. Importantly, *Chsy* mutants showed a single or co-occurrence of these defects, suggesting a possible interconnection behind these mutant phenotypes. Further, apicobasal polarity of the developing follicle cell epithelia and their adhesion to the germline cysts are compromised. Finally, proper specification of the stalk cell fate is compromised and the BM becomes morphologically disorganized in the *Chsy* mutant ovarioles. Hence, we hypothesize that the combination of these observed phenotypes synergistically leads to a subsequent breakdown of the gross organ architecture.

Altogether, our study reveals that normal CS biosynthesis is required for the proper organ development and maintenance, as well as the BM integrity. The initial assembly of the organ can occur in the absence of *Chsy,* but it is likely that normal CS function is required for the maintenance of the structural integrity of the ECM and gross organ architecture. Moreover, although associations behind the mechanism of observed defects may be possible, further work on the underlying connection between the overlapping defects will help establish the global function of CS during organ development and maintenance.

Materials and Methods

Drosophila strains

The following fly strains were used in this study: Oregon-R, *Chsy*^{1}, and *Chsy*^{2}. Flies were raised on a standard cornmeal fly medium at 25°C unless otherwise indicated. *Chsy*^{1} and *Chsy*^{2} mutant flies are generated by CRISPR-Cas9 mutagenesis described below. All flies are fed with yeast powder two days prior to dissection and analysis.

CRISPR-Cas9 Mutagenesis

Chsy^{1} and *Chsy*^{2} alleles were generated as previously described, but CRISPR-Cas9-mediated nonhomologous end joining (NHEJ) was utilized instead of homology-directed repair (HDR) (Takemura and Nakato, 2017). In short, combinations of two sgRNA-containing plasmids were injected into the yw; nos-Cas9(y+)/CyO strain to delete portions of the *Chsy* gene and repair by NHEJ, then were crossed with y+ w- dSmad2 {W+ E0348} / FM7 {*ActGFP*}. Resultant recombinants were screened via PCR and verified by Sanger sequencing, followed by backcrossing with Oregon-R strain.

Preparation of adult wings

The right wings from flies were dehydrated in ethanol and subsequently with xylene {Fujise, 2001 #2}{Takemura, 2020 #32}. The specimens were mounted in Canada balsam (Benz Microscope, BB0020).

Reproductive ability and quality analysis

Twenty-five mating pairs (25 male and 25 female adult flies) at ages of interest are selected and placed in the apparatus for analysis. The apparatus was set up as the following: selected flies were put into a fly-cage with holes for air ventilation and a grape-juice plate streaked with yeast paste was placed on top. The apparatus was then flipped upside down with the grape-juice plate on the bottom and flies were nurtured at 25°C for 24 hours prior to the actual collection of eggs for adjustment to the new environment. At the start of the experiment, old grape juice plate was discarded and replaced with a new grape juice plate streaked with yeast paste for the collection of eggs. Plates were switched every 3 hours until 3 plates (9 hours total) were collected for each analysis and the number of laid eggs was counted for each plate under the microscope. Following the counting of eggs, they were raised in the same plates at 25°C until they hatched, and the number of hatched eggs was counted for each plate under the microscope.

Immunohistochemstry analysis

Immunostaining of the ovaries was performed as previously described with some modifications {Takemura, 2020}{Hayashi, 2009; Hayashi, 2012}. In short, dissected ovaries were fixed for 20 minutes with 4% formaldehyde in PBS and washed with 0.1% PBST (0.1% Triton X-100 in PBS) for 30 minutes (10 minutes, three times). They were then blocked in 5% normal goat serum in 0.1% PBST for one hour, and incubated overnight in primary antibodies at 4ºC. Samples were again washed in 0.1% PBST (10 minutes, three times) and incubated with secondary antibodies either overnight at 4°C or for two hours at room temperature. They were washed in 0.1% PBST (10 minutes, three times), before being mounted in either 80% glycerol in PBS or VECTASHIELD (H-1000

or H-1200, Vector Laboratory). Images were obtained using a Zeiss 710 laser scanning confocal microscope.

The primary antibodies used were as follows: mouse anti-Fasciclin III 7G10 (1:50, Developmental Studies Hybridoma Bank [DSHB]), mouse anti-LaminC LC28.26 (1:100, DSHB), rabbit anti-Vasa (1:50, a gift from S. Kobayashi), mouse anti-Armadillo-s N27A1(1:100, DSHB), and rabbit anti-Viking (1:2000, a gift from Stéphane Noselli). Alexa488, Alexa568, and Alexa633-conjugated secondary antibodies (Thermo Fisher Scientific) were used at a dilution of 1:200.

Disaccharide analysis

CS isolation and disaccharide composition analysis were carried out as previously described {Toyoda, 2000 #9}{Kamimura, 2006 #19}{Kleinschmit, 2010 #4}{Dejima, 2013 #44}{Nakato, 2019 #46}. Approximately 5 mg of adult flies were used to isolate CS. The CS sample was digested with condroitinase ABC, and the resulting disaccharide species were separated using reversed-phase ion-pair chromatography. The effluent was monitored fluorometrically for post-column detection of HS disaccharides {Toyoda, 2000 #9}.

Figures and Figure Legends

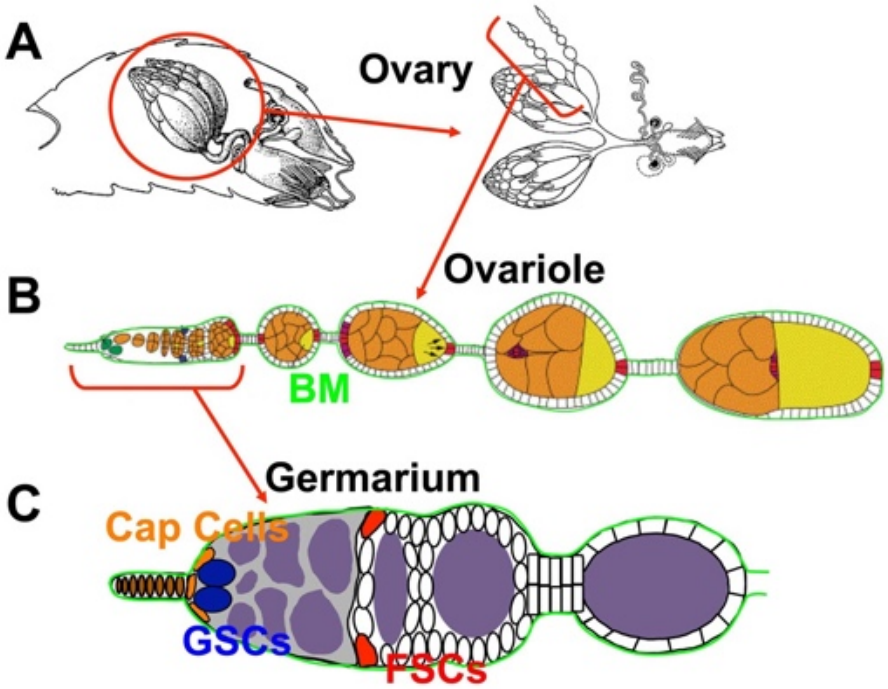

Fig. 1. The anatomy of the Drosophila ovary.
(A) The *Drosophila* ovary is composed of 16–20 ovarioles. (B) Each ovariole contains progressively developing egg chambers. The developing germ cells are surrounded by different types of follicle cells. The ovariole is enwrapped by BM (thin green line). (C) At the anterior tip of each ovariole, a structure called the germarium contains the two populations of stem cells, germline stem cells (GSC, blue) and follicle stem cells (FSC, red). Cap cells (orange) directly contact with and serve as niche cells for GSCs. Figure is modified from FlyBase images.

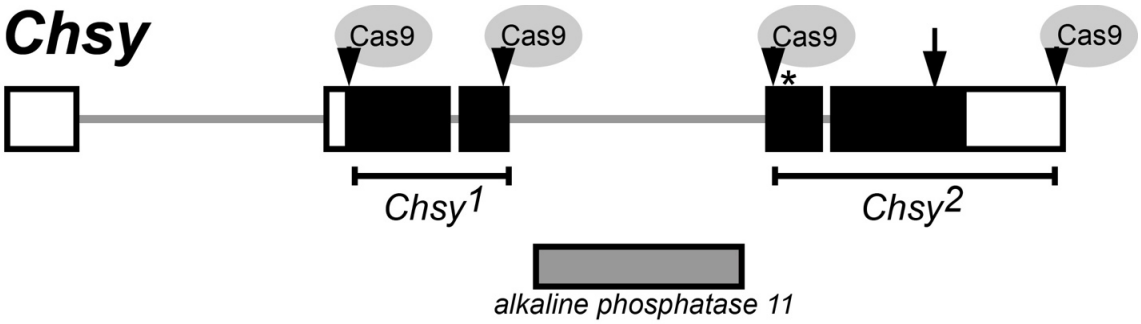

Fig. 2. Organization of the *Chsy* locus and generation of *Chsy* mutant alleles.
A schematic of the *Chsy* locus and the generation of two null mutations, *Chsy*^{1} and *Chsy*^{2}, using the CRISPR–Cas9 system, one on each side of intronic *alkaline phosphatase 11* gene. The arrow shows the position of the enzyme catalytic site, and the asterisk shows the position of a methionine residue.

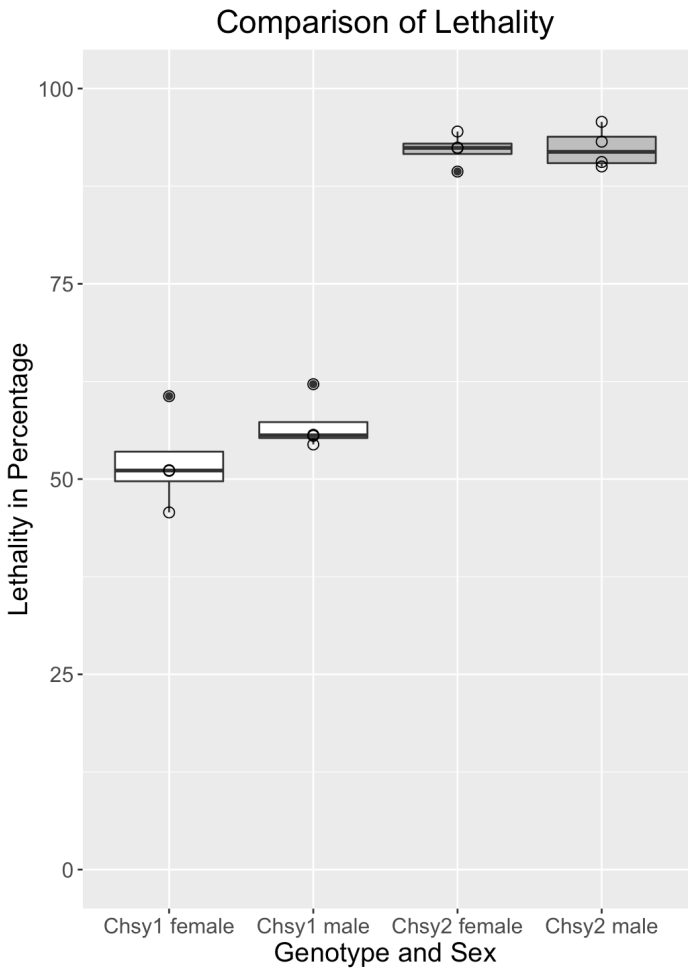

Fig. 3. Lethality profiles of mutants with *Chsy*^{1} vs. *Chsy*^{2} alleles.
Quantification of the average lethality rate in percentage for each respective genotype and sex. See Table 1 for the represented values.

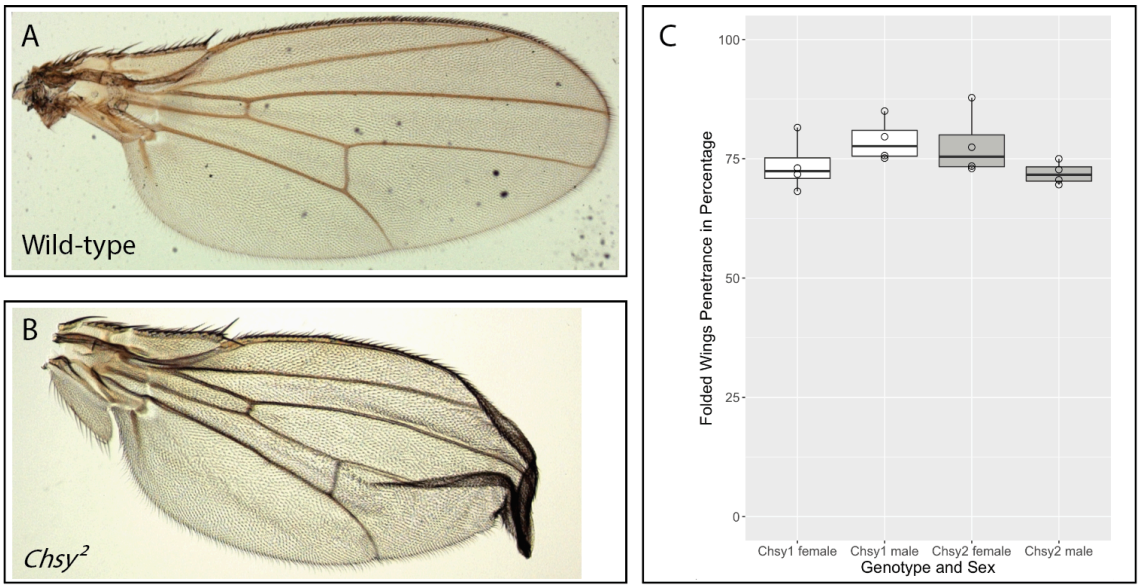

Fig. 4. Folded-wing phenotype and its penetrance in *Chsy* mutants.
(A) Representative light microscopy image of a right-wing from wild-type control animals at 5x magnification. (B) Representative light microscopy image of a right-wing from mutant animals containing the *Chsy*^{2} allele at 5x magnification. (C) Quantification of the average folded-wing phenotype penetrance in percentage for each respective genotype and sex. See Table 2 for the represented values.

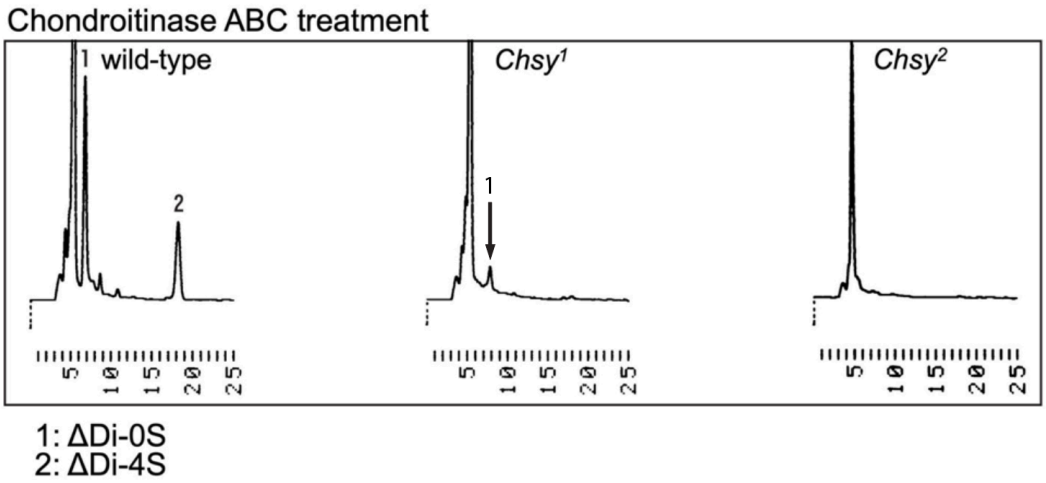

Fig. 5. HPLC profiles of CS disaccharides from wild-type and *Chsy* mutants. Chromatograms of unsaturated disaccharides from wild-type (left), Chsy1 (middle) and Chsy2 (right) mutant adult flies. After CS was completely digested with condroitinase ABC, the resultant disaccharide species were separated by reversed-phase ion-pair chromatography (Docosil C22) with post-column detection system. Peaks for the two disaccharides ΔDi-0S (1) and ΔDi-4S (2) are shown for wild-type.

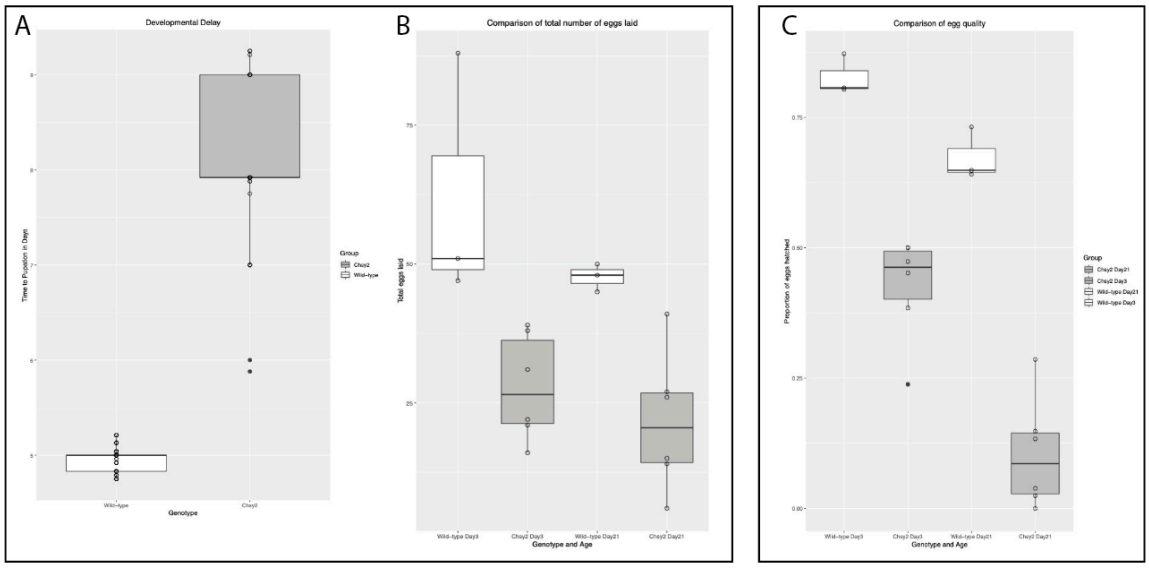

Fig. 6. Statistics of developmental delay and egg quality defects in *Chsy* mutants. (A) Quantification of the average time taken from egg to pupation in days for each respective genotype. (B) Quantification of the average number of total eggs laid over 3hr period for each respective genotype and age of female parents. (C) Quantification of the average proportion of eggs hatched for each respective genotype and age of female parents. For A-C, see Table 3 for the represented values. Boxplots shaded in white and gray represent data for wild-type and *Chsy* mutant animals, respectively.

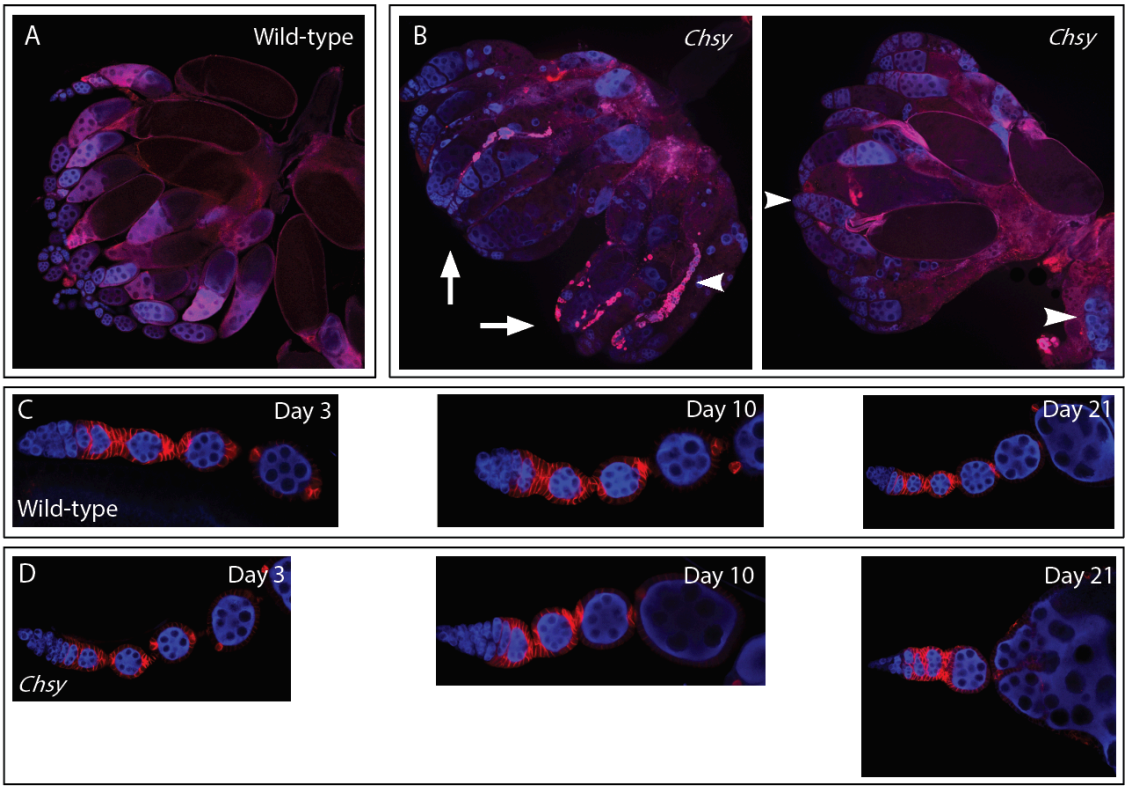

Fig. 7. Morphology comparison of wild-type vs. *Chsy* mutant whole ovaries and ovarioles.
(A-B) Immunofluorescent (IF) staining for FasIII (red, marking follicle cells) and Vasa (blue, marking germ cells) in the wild-type control (A) versus *Chsy* mutant (B) whole ovaries. In B, arrows indicate altered morphology of *Chsy* mutant ovaries with decreased size and arrowheads indicate non-spatiotemporally ordered alignment of developing egg chambers during oogenesis. (C-D) IF staining for FasIII (red) and Vasa (blue) in the wild-type (C) versus *Chsy* mutant (D) ovarioles at different ages. In D, gradual deterioration in the structural integrity of *Chsy* mutant ovarioles with age progression is represented. Severe morphological defects are shown in the ovarioles of old (day-21 post eclosion) *Chsy* mutants. IF images for whole ovaries are taken at 10x magnification and those for ovarioles are taken at 40x total magnification.

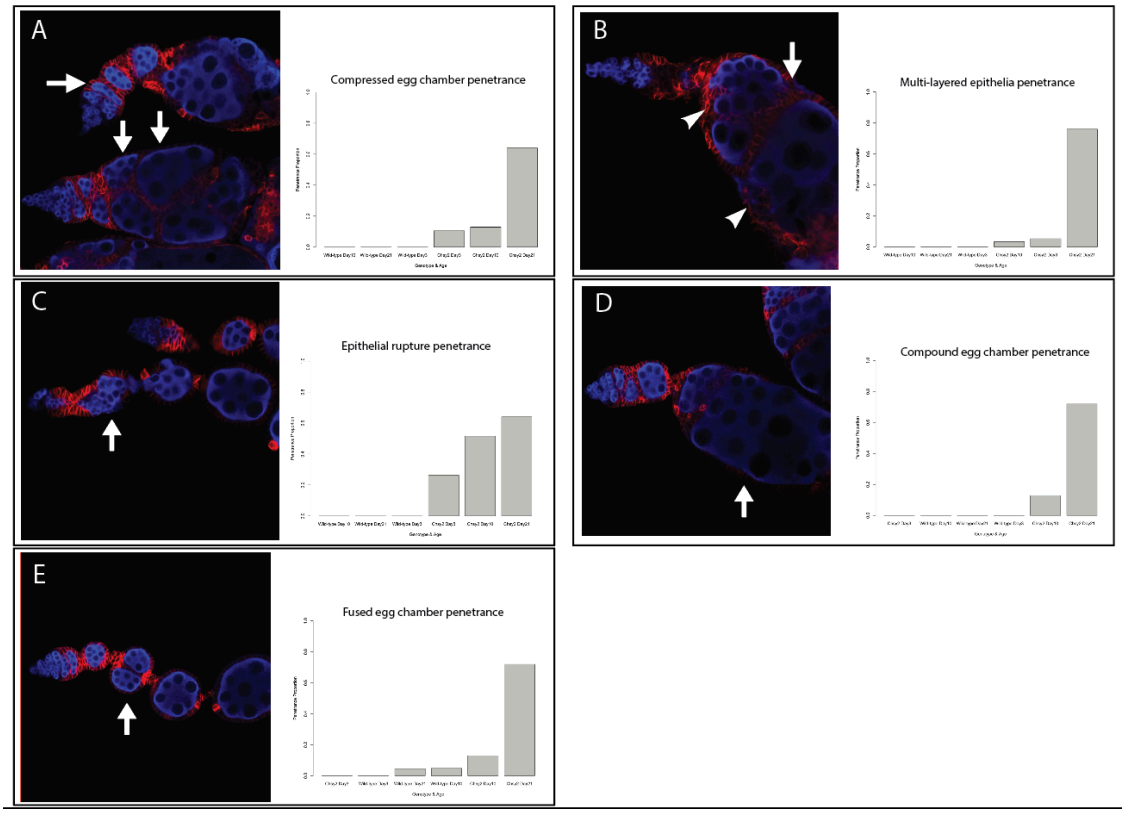

Fig. 8. Distinctive phenotypic abnormalities in the *Chsy* mutant ovarioles.
(A-E) IF staining for FasIII (red) and Vasa (blue) showing five distinctive phenotypic defects in the *Chsy* mutant ovarioles at day-21 post eclosion. Penetrance comparisons between the wild-type control and *Chsy* mutant animals at young, mid, and old ages (day-3, -10, and -21, respectively) are shown for all defective categories in the right of each representative image, and the values are given as proportions. (A) Representative image of the *Chsy* mutant ovariole showing the 'compressed' egg chamber phenotype (arrows). Penetrance is increased from 10.53% and 12.90% at day-3 and -10, respectively, to 64% at day-21 in the *Chsy* mutants. (B) Representative image of the *Chsy* mutant ovariole showing the 'multi-layered epithelia' phenotype. Arrow indicates multi-layered epithelia and arrowheads indicate ingression of epithelial clusters into germline cysts. Penetrance is increased from 5.26% and 3.23% at day-3 and -10, respectively, to 76% at day-21 in the *Chsy* mutants. (C) Representative image of the *Chsy* mutant ovariole showing the 'epithelial rupture' phenotype (arrow). Penetrance is increased from 26.32% and 51.61% at day-3 and -10, respectively, to 64% at day-21 in the *Chsy* mutants. (D) Representative image of the *Chsy* mutant ovariole showing the 'compound' egg chamber phenotype (arrow). Penetrance is increased from 0% and 12.90% at day-3 and -10, respectively, to 72% at day-21 in the *Chsy* mutants. (E) Representative image of the *Chsy* mutant ovariole showing the 'fused' egg chamber phenotype (arrow). Penetrance is increased from 0% and 12.90% at day-3 and -10, respectively, to 72% at day-21 in the *Chsy* mutants. All IF images are taken at 40x magnification total. Total of 19, 21, and 22 ovariole samples are analyzed for wild-type flies at day-3, -10, and -21 post eclosion, respectively. Total of 19, 31, and 25 ovariole samples are analyzed for *Chsy* mutant flies at day-3, -10, and -21 post eclosion, respectively.

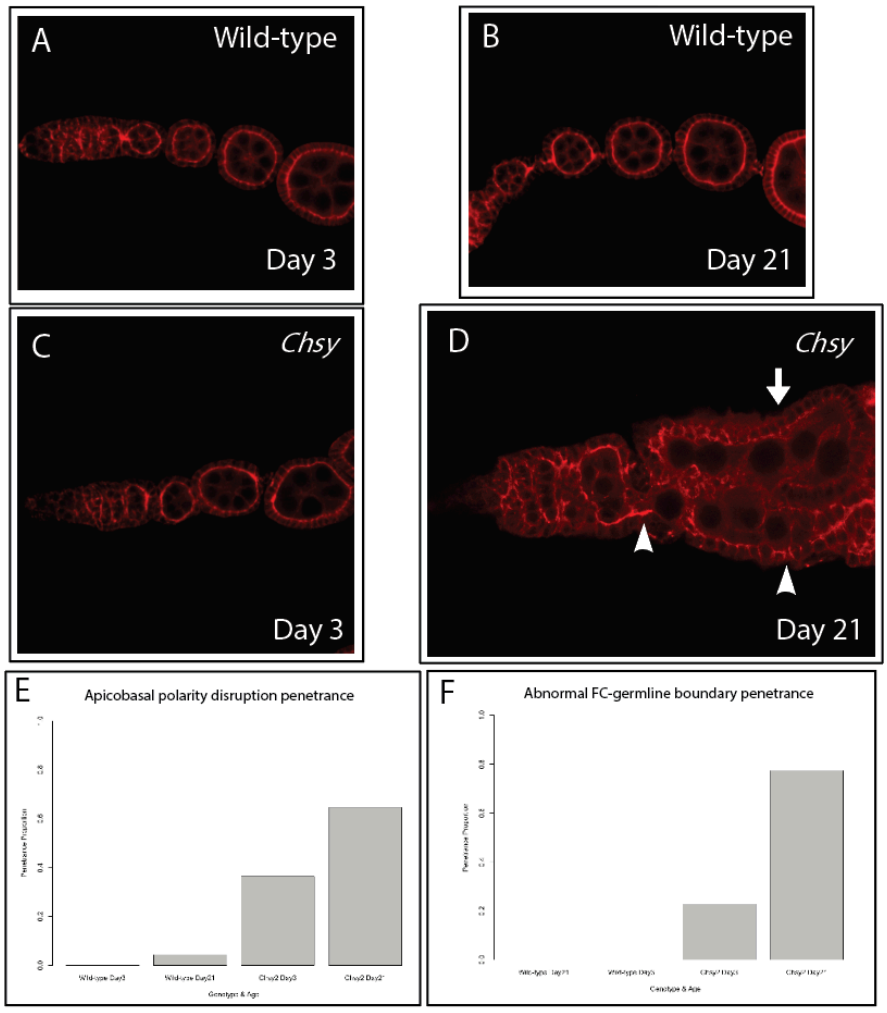

Fig. 9. Compromised apicobasal polarity of follicle cell epithelia in the *Chsy* mutant ovarioles.

(A-D) IF staining for Armadillo (Arm) (red, marking adherens junctions) in the young and old wild-type control (A-B) versus young and old *Chsy* mutant (C-D) ovarioles. (A-B) Arm is properly localized in the ovarioles of wild-type flies at both ages. (C-D) Arm is properly localized in most ovarioles of the young *Chsy* mutant flies (C), but its localization gets severely compromised as mutant animals age (D). In D, arrowheads indicate examples of the disruption in apicobasal polarity and arrow indicates an egg chamber example with compromised FC-germline boundaries in the old *Chsy* mutant ovarioles. (E-F) Penetrance comparisons are shown for the phenotypes of apicobasal polarity disruption (E) and abnormal FC-germline boundary (F) between the wild-type and *Chsy* mutant animals at different ages, and the values are given as proportions. In E, penetrance of apicobasal polarity disruption is increased from 36.36% at day-3 to 64.52% at day-21 in the *Chsy* mutants. In F, penetrance of abnormal FC-germline boundary is increased from 22.73% at day-3 to 77.42% at day-21 in the *Chsy* mutants. All IF images are taken at 40x magnification total. Total of 22 and 23 ovariole samples are analyzed for wild-type flies at day-3 and -21 post eclosion, respectively. Total of 22 and 31 ovariole samples are analyzed for *Chsy* mutant flies at day-3 and -21 post eclosion, respectively.

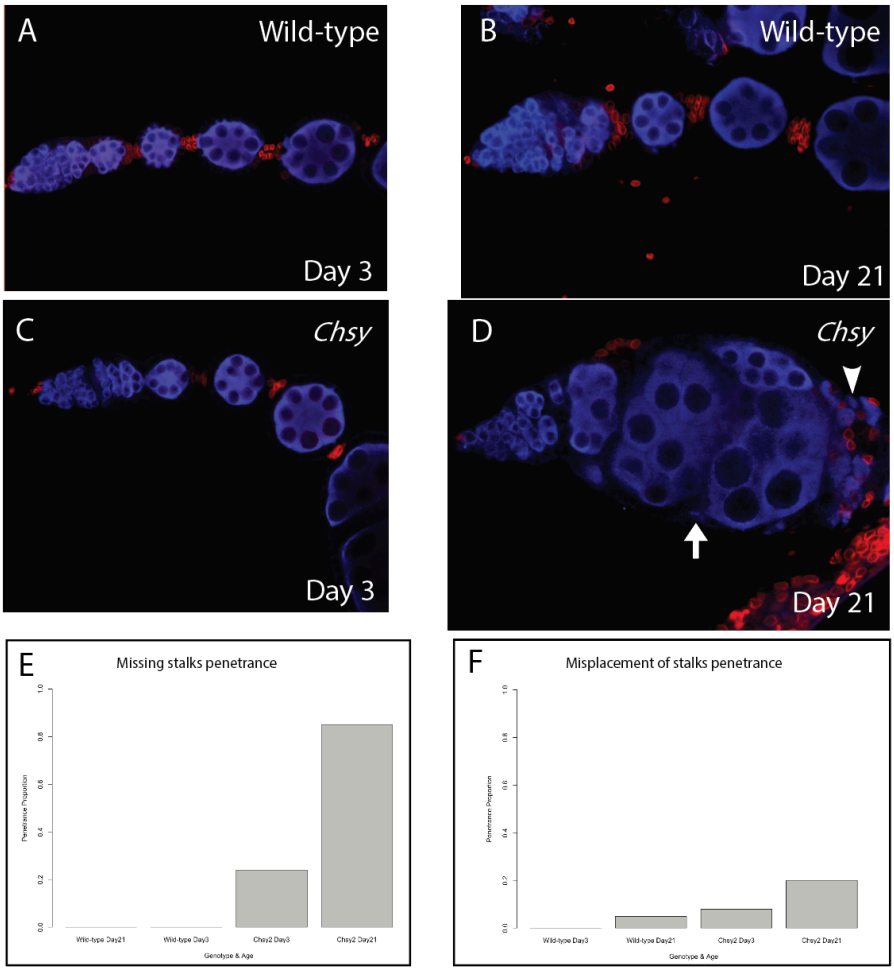

Fig. 10. Improper specification of stalk cell fate in the *Chsy* mutant ovarioles. (A-D) IF staining for Lamin C (red, marking stalk cells) and Vasa (blue) in the young and old wild-type control (A-B) versus young and old *Chsy* mutant (C-D) ovarioles. (A-B) Normal specification of stalk cell fate is observed in the ovarioles of wild-type flies at both ages. (C-D) Increased cases of defects in the stalk cell fate specification are observed with age progression in the ovarioles of *Chsy* mutant animals. In D, arrow indicates an example of the abolished stalk formation and arrowhead indicates an example of the misplacement of stalk cells in the old *Chsy* mutant ovarioles. (E-F) Penetrance comparisons are shown for the defects of compromised stalk formations (E) and misplacement of stalk cells (F) between the wild-type and *Chsy* mutant animals at different ages, and the values are given as proportions. In E, penetrance of no formation of stalks is increased from 24% at day-3 to 85% at day-21 in the *Chsy* mutants. In F, penetrance of the misplacement of stalk cells is increased from 8% at day-3 to 20% at day-21 in the *Chsy* mutants. All IF images are taken at 40x magnification total. Total of 30 and 20 ovariole samples are analyzed for wild-type flies at day-3 and -21 post eclosion, respectively. Total of 25 and 20 ovariole samples are analyzed for *Chsy* mutant flies at day-3 and -21 post eclosion, respectively.

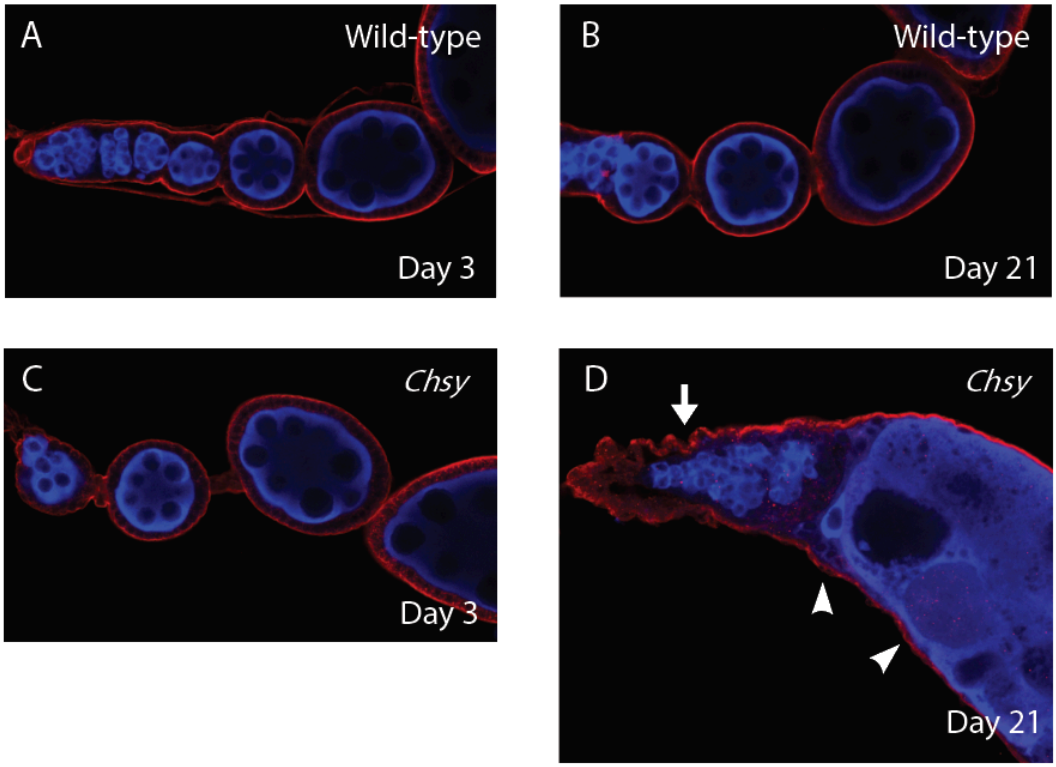

Fig. 11. Disorganization of the BM morphology in the *Chsy* mutant ovarioles. (A-D) IF staining for Viking (Vkg) (red, marking ColIV of the BM) and Vasa (blue) in the young and old wild-type control (A-B) versus young and old *Chsy* mutant (C-D) ovarioles. (A-B) Normal BM morphology is observed in the ovarioles of wild-type flies at both ages. (C-D) BM appears normal in the ovarioles of young *Chsy* mutants (C), but is morphologically disorganized at day-21 after eclosion with alterations in the gross ovariole architecture (D). In D, arrow indicates an example of the morphologically disorganized BM and arrowheads indicate examples of the 'chain-like' BM with interstices in the old *Chsy* mutant ovarioles. All IF images are taken at 40x magnification total.

Tables

	***Chsy*^{1} Female**	***Chsy*^{1} Male**	***Chsy*^{2} Female**	***Chsy*^{2} Male**
Average Lethality Rate, %	52.13 ± 6.19	56.94 ± 3.51	92.17 ± 2.11	92.39 ± 2.63

Table 1. Average lethality rate of mutants with *Chsy*^{1} vs. *Chsy*^{2} alleles.
Average lethality rate is shown for each respective genotype and sex. The values are given as percentage of non-survivors divided by total number of samples, and represent mean lethality rates ± S.D. Total number of samples were 1660, 1336, 2051, and 1921 for *Chsy*^{1} female, *Chsy*^{1} male, *Chsy*^{2} female, *Chsy*^{2} male, respectively. Graphical depiction of the results is shown in Fig.3.

	***Chsy*^{1} Female**	***Chsy*^{1} Male**	***Chsy*^{2} Female**	***Chsy*^{2} Male**
Average folded-wing phenotype penetrance, %	73.64 ± 5.66	78.86 ± 4.56	77.92 ± 6.89	71.97 ± 2.41

Table 2. Average folded-wing phenotype penetrance of mutants with *Chsy*^{1} vs. *Chsy*^{2} alleles.
Average folded-wing phenotype penetrance is shown for each respective genotype and sex. The values are given as percentage of animals showing the folded-wing phenotype from total number of animals evaluated, and represent mean percentages of penetrance ± S.D. Total number of samples were 1660, 1336, 2051, and 1921 for *Chsy*^{1} female, *Chsy*^{1} male, *Chsy*^{2} female, *Chsy*^{2} male, respectively. Graphical depiction of the results is shown in Fig.4.

	Genotype	
	Wild-type	**Chsy2**
Average Time to Pupation in Days	4.96 ± 0.12	8.11 ± 0.85
p-values from ANOVA (Wild-type-Chsy2)	2e-16 ***	

Table 3A

	Wild-type Day 3	**Chsy2 Day 3**	**Wild-type Day 21**	**Chsy2 Day 21**
Average Number of Total Eggs Laid in 3 hrs	62.00 ± 22.61	27.83 ± 9.58	47.67 ± 2.52	21.50 ± 12.41

p-values for comparisons showing statistical significance	Wild-type Day21 – *Chsy²* Day21 0.05 ’	Wild-type Day3 – *Chsy²* Day21 0.002 *	Wild-type Day3 – *Chsy²* Day3 0.009 *

Table 3B

	Wild-type Day 3	**Chsy2 Day 3**	**Wild-type Day 21**	**Chsy2 Day 21**
Average Proportion of Eggs Hatched	0.83 ± 0.04	0.42 ± 0.10	0.67 ± 0.05	0.11 ± 0.11

p-values for comparisons showing statistical significance	*Chsy²* Day3 – *Chsy²* Day21 1.5e-4 **	Wild-type Day21 – *Chsy²* Day21 2.3e-6 ***	Wild-type Day3 – *Chsy²* Day3 1.1e-4 **	Wild-type Day3 – *Chsy²* Day21 & Wild-type Day21 – *Chsy²* Day3 1e-7 *** & 0.008 *

Table 3C

Table 3. Average data of developmental delay and egg quality defects in *Chsy* mutants. (A) Average time from egg to pupation is shown for both genotypes in days. Total of 106 wild-type and 43 *Chsy²* pupae were sampled in the analysis. The values are given as mean number of days taken ± S.D. p-value for statistical significance between two genotypes is shown. (B) Average number of total eggs laid over 3hr period is shown for each respective genotype and age of female parents that laid eggs. Collection of eggs were repeated 6 times for the *Chsy²* mutants and 3 times for the wild-type animals under same conditions. Over 150 eggs are collected in total for the analysis of all genotypes and age and are used for the subsequent analysis of egg quality. The values are given as mean number of total eggs laid during the 3hr duration ± S.D. and table of p-values for comparisons that showed statistical significance is also shown. (C) Average values for the proportion of eggs hatched is shown for each genotype and age of female parents that laid eggs. Total number of samples and replicates are same as the previous analysis of egg laying experiment. The values are given as proportion of eggs hatched from total number of eggs analyzed ± S.D. and table of p-values for comparisons that showed statistical significance is shown. ‘P<0.05; *P<0.01; **P<0.001; ***P<0 (one-way ANOVA for all data sets in table 3). Graphical depiction of the results is shown in Fig.6.

References

Akiyama, T., Kamimura, K., Firkus, C., Takeo, S., Shimmi, O., & Nakato, H. (2008). Dally regulates Dpp morphogen gradient formation by stabilizing Dpp on the cell surface. *Developmental biology*, *313*(1), 408–419. https://doi.org/10.1016/j.ydbio.2007.10.035

Bäumer, D., Ströhlein, N.M. & Schoppmeier, M. Opposing effects of Notch-signaling in maintaining the proliferative state of follicle cells in the telotrophic ovary of the beetle *Tribolium*. *Front Zool* **9,** 15 (2012). https://doi.org/10.1186/1742-9994-9-15

Belenkaya, T. Y., Han, C., Yan, D., Opoka, R. J., Khodoun, M., Liu, H., & Lin, X. (2004). Drosophila Dpp morphogen movement is independent of dynamin-mediated endocytosis but regulated by the glypican members of heparan sulfate proteoglycans. *Cell*, *119*(2), 231–244. https://doi.org/10.1016/j.cell.2004.09.031

Bellaiche, Y., The, I., & Perrimon, N. (1998). Tout-velu is a Drosophila homologue of the putative tumour suppressor EXT-1 and is needed for Hh diffusion. *Nature*, *394*(6688), 85–88. https://doi.org/10.1038/27932

Berns, N., Woichansky, I., Friedrichsen, S., Kraft, N., & Riechmann, V. (2014). A genome-scale in vivo RNAi analysis of epithelial development in Drosophila identifies new proliferation domains outside of the stem cell niche. *Journal of cell science*, *127*(Pt 12), 2736–2748. https://doi.org/10.1242/jcs.144519

Bilousov, O. O., Kozeretska, I. A., & Katanaev, V. L. (2012). Role of the gene Miniature in Drosophila wing maturation. *Genesis (New York, N.Y. : 2000)*, *50*(7), 525–533. https://doi.org/10.1002/dvg.22016

Bowden, N. and Nakato, H. (2021). Heparan Sulfate Proteoglycans in the Stem Cell Niche: Lessons from Drosophila. In "Proteoglycans in stem cells: From development to cancer." 1-19. (Eds. by Götte, M. and Forsberg-Nilsson, K., Springer Nature)

Cetera, M., Ramirez-San Juan, G. R., Oakes, P. W., Lewellyn, L., Fairchild, M. J., Tanentzapf, G., Gardel, M. L., & Horne-Badovinac, S. (2014). Epithelial rotation promotes the global alignment of contractile actin bundles during Drosophila egg chamber elongation. *Nature communications*, *5*, 5511. https://doi.org/10.1038/ncomms6511

Chanet, S., & Huynh, J. R. (2020). Collective Cell Sorting Requires Contractile Cortical Waves in Germline Cells. *Current biology : CB*, *30*(21), 4213–4226.e4. https://doi.org/10.1016/j.cub.2020.08.045

Crest, J., Diz-Munõ z, A., Chen, D.-Y., Fletcher, D. A. and Bilder, D. (2017). Organ sculpting by patterned extracellular matrix stiffness. Elife 6, 1-16. doi:10.7554/ eLife.24958

Daley, W. P. and Yamada, K. M. (2013). ECM-modulated cellular dynamics as a driving force for tissue morphogenesis. Curr. Opin. Genet. Dev. 23, 408-414. doi:10.1016/j.gde.2013.05.005

Dejima, K., Kleinschmit, A., Takemura, M., Choi, P. Y., Kinoshita-Toyoda, A., Toyoda, H., & Nakato, H. (2013). The role of Drosophila heparan sulfate 6-O-endosulfatase in sulfation compensation. *The Journal of biological chemistry*, *288*(9), 6574–6582. https://doi.org/10.1074/jbc.M112.404830

Diaz-Torres, A., Rosales-Nieves, A.E., Pearson, J.R., Santa-Cruz Mateos, C., Marin-Menguiano, M., Marshall, O.J., Brand, A.H., and Gonzalez-Reyes, A. (2021). Stem cell niche organization in the Drosophila ovary requires the ECM component Perlecan. Curr Biol *31*, 1744-1753 e1745.

Esko, J. D., & Selleck, S. B. (2002). Order out of chaos: assembly of ligand binding sites in heparan sulfate. *Annual review of biochemistry*, *71*, 435–471. https://doi.org/10.1146/annurev.biochem.71.110601.135458

Fernández-Miñán, A., Martín-Bermudo, M. D., & González-Reyes, A. (2007). Integrin signaling regulates spindle orientation in Drosophila to preserve the follicular-epithelium monolayer. *Current biology : CB*, *17*(8), 683–688. https://doi.org/10.1016/j.cub.2007.02.052

Franz A., Riechmann V. (2010). Stepwise polarisation of the Drosophila follicular epithelium. *Dev. Biol.* 338, 136–147. https://doi.org/10.1016/j.ydbio.2009.11.027

Fujise, M., Takeo, S., Kamimura, K., Matsuo, T., Aigaki, T., Izumi, S., & Nakato, H. (2003). Dally regulates Dpp morphogen gradient formation in the Drosophila wing. *Development (Cambridge, England)*, *130*(8), 1515–1522. https://doi.org/10.1242/dev.00379

Gates J. (2012). Drosophila egg chamber elongation: insights into how tissues and organs are shaped. *Fly*, *6*(4), 213–227. https://doi.org/10.4161/fly.21969

Georgiou, M., Marinari, E., Burden, J., & Baum, B. (2008). Cdc42, Par6, and aPKC regulate Arp2/3-mediated endocytosis to control local adherens junction stability. *Current biology : CB*, *18*(21), 1631–1638. https://doi.org/10.1016/j.cub.2008.09.029

Guo, Z., & Wang, Z. (2009). The glypican Dally is required in the niche for the maintenance of germline stem cells and short-range BMP signaling in the Drosophila ovary. *Development (Cambridge, England)*, *136*(21), 3627–3635. https://doi.org/10.1242/dev.036939

Haigo, S. L., & Bilder, D. (2011). Global tissue revolutions in a morphogenetic movement controlling elongation. *Science (New York, N.Y.)*, *331*(6020), 1071–1074. https://doi.org/10.1126/science.1199424

Harris, K. P., & Tepass, U. (2008). Cdc42 and Par proteins stabilize dynamic adherens junctions in the Drosophila neuroectoderm through regulation of apical endocytosis. *The Journal of cell biology*, *183*(6), 1129–1143. https://doi.org/10.1083/jcb.200807020

Hayashi, Y., Kobayashi, S., and Nakato, H. (2009). Drosophila glypicans regulate the germline stem cell niche. J Cell Biol *187*, 473-480.

He, L., Wang, X., Tang, H. L., & Montell, D. J. (2010). Tissue elongation requires oscillating contractions of a basal actomyosin network. *Nature cell biology*, *12*(12), 1133–1142. https://doi.org/10.1038/ncb2124

Herman, T., Hartwieg, E., and Horvitz, H.R. (1999). sqv mutants of Caenorhabditis elegans are defective in vulval epithelial invagination. Proc Natl Acad Sci U S A *96*, 968-973.

Hongay, C. F., & Orr-Weaver, T. L. (2011). Drosophila Inducer of MEiosis 4 (IME4) is required for Notch signaling during oogenesis. *Proceedings of the National Academy of Sciences of the United States of America*, *108*(36), 14855–14860. https://doi.org/10.1073/pnas.1111577108

Howard, A. M., LaFever, K. S., Fenix, A. M., Scurrah, C. R., Lau, K. S., Burnette, D. T., Bhave, G., Ferrell, N., & Page-McCaw, A. (2019). DSS-induced damage to basement membranes is repaired by matrix replacement and crosslinking. *Journal of cell science*, *132*(7), jcs226860.

Isabella, A. J. and Horne-Badovinac, S. (2016). Rab10-mediated secretion synergizes with tissue movement to build a polarized basement membrane architecture for organ morphogenesis. Dev. Cell 38, 47-60. doi:10.1016/j.devcel. 2016.06.009

Isabella, A. J., & Horne-Badovinac, S. (2015). Building from the Ground up: Basement Membranes in Drosophila Development. *Current topics in membranes*, *76*, 305–336. https://doi.org/10.1016/bs.ctm.2015.07.001

Kamimura, K., Koyama, T., Habuchi, H., Ueda, R., Masu, M., Kimata, K., & Nakato, H. (2006). Specific and flexible roles of heparan sulfate modifications in Drosophila FGF signaling. *The Journal of cell biology*, *174*(6), 773–778. https://doi.org/10.1083/jcb.200603129

Kiger, J. A., Jr, Natzle, J. E., & Green, M. M. (2001). Hemocytes are essential for wing maturation in Drosophila melanogaster. *Proceedings of the National Academy of Sciences of the United States of America*, *98*(18), 10190–10195. https://doi.org/10.1073/pnas.181338998

Kiger, J. A., Jr, Natzle, J. E., Kimbrell, D. A., Paddy, M. R., Kleinhesselink, K., & Green, M. M. (2007). Tissue remodeling during maturation of the Drosophila wing. *Developmental biology*, *301*(1), 178–191. https://doi.org/10.1016/j.ydbio.2006.08.011

Kirkpatrick, C.A., and Selleck, S.B. (2007). Heparan sulfate proteoglycans at a glance. J Cell Sci *120*, 1829-1832.

Kleinschmit, A., Koyama, T., Dejima, K., Hayashi, Y., Kamimura, K., & Nakato, H. (2010). Drosophila heparan sulfate 6-O endosulfatase regulates Wingless morphogen gradient formation. *Developmental biology*, *345*(2), 204–214. https://doi.org/10.1016/j.ydbio.2010.07.006

Leibfried, A., Fricke, R., Morgan, M. J., Bogdan, S., & Bellaiche, Y. (2008). Drosophila Cip4 and WASp define a branch of the Cdc42-Par6-aPKC pathway regulating E-cadherin endocytosis. *Current biology : CB*, *18*(21), 1639–1648. https://doi.org/10.1016/j.cub.2008.09.063

Li, Y., Laue, K., Temtamy, S., Aglan, M., Kotan, L.D., Yigit, G., Canan, H., Pawlik, B., Nurnberg, G., Wakeling, E.L.*, et al.* (2010). Temtamy preaxial brachydactyly syndrome is caused by loss-of-function mutations in chondroitin synthase 1, a potential target of BMP signaling. Am J Hum Genet *87*, 757-767.

Lin, X., Buff, E. M., Perrimon, N., & Michelson, A. M. (1999). Heparan sulfate proteoglycans are essential for FGF receptor signaling during Drosophila embryonic development. *Development (Cambridge, England)*, *126*(17), 3715–3723. https://doi.org/10.1242/dev.126.17.3715

Lindahl, U., & Li, J. P. (2009). Interactions between heparan sulfate and proteins-design and functional implications. *International review of cell and molecular biology*, *276*, 105–159. https://doi.org/10.1016/S1937-6448(09)76003-4

Lovegrove, H. E., Bergstralh, D. T., & St Johnston, D. (2019). The role of integrins in *Drosophila* egg chamber morphogenesis. *Development (Cambridge, England)*, *146*(23), dev182774. https://doi.org/10.1242/dev.182774

Lu, H., & Bilder, D. (2005). Endocytic control of epithelial polarity and proliferation in Drosophila. *Nature cell biology*, *7*(12), 1232–1239. https://doi.org/10.1038/ncb1324

Ma, M., Cao, X., Dai, J., and Pastor-Pareja, J.C. (2017). Basement Membrane Manipulation in Drosophila Wing Discs Affects Dpp Retention but Not Growth Mechanoregulation. Dev Cell *42*, 97-106 e104.

Matthew Antel, Taylor Simao, Muhammed Burak Bener, Mayu Inaba. bioRxiv 2021.06.07.447432; doi: https://doi.org/10.1101/2021.06.07.447432

Mikami, T., and Kitagawa, H. (2013). Biosynthesis and function of chondroitin sulfate. Biochim Biophys Acta *1830*, 4719-4733.

Mizuguchi, S., Uyama, T., Kitagawa, H., Nomura, K.H., Dejima, K., Gengyo-Ando, K., Mitani, S., Sugahara, K., and Nomura, K. (2003). Chondroitin proteoglycans are involved in cell division of Caenorhabditis elegans. Nature *423*, 443-448.

Morrison, H. A., Dionne, H., Rusten, T. E., Brech, A., Fisher, W. W., Pfeiffer, B. D., Celniker, S. E., Stenmark, H., & Bilder, D. (2008). Regulation of early endosomal entry by the Drosophila tumor suppressors Rabenosyn and Vps45. *Molecular biology of the cell*, *19*(10), 4167–4176. https://doi.org/10.1091/mbc.e08-07-0716

Morrissey, M. A. and Sherwood, D. R. (2015). An active role for basement membrane assembly and modification in tissue sculpting. J. Cell Sci. 128, 1661-1668. doi:10.1242/jcs.168021

Nakato, E., Liu, X., Eriksson, I., Yamamoto, M., Kinoshita-Toyoda, A., Toyoda, H., Kjellén, L., Li, J. P., & Nakato, H. (2019). Establishment and characterization of Drosophila cell lines mutant for heparan sulfate modifying enzymes. *Glycobiology*, *29*(6), 479–489. https://doi.org/10.1093/glycob/cwz020
Nakato, H., and Li, J.P. (2016). Functions of Heparan Sulfate Proteoglycans in Development: Insights From Drosophila Models. Int Rev Cell Mol Biol *325*, 275-293.

Noborn, F., Gomez Toledo, A., Nasir, W., Nilsson, J., Dierker, T., Kjellen, L., and Larson, G. (2018). Expanding the chondroitin glycoproteome of Caenorhabditis elegans. J Biol Chem *293*, 379-389.

Olson, S.K., Bishop, J.R., Yates, J.R., Oegema, K., and Esko, J.D. (2006). Identification of novel chondroitin proteoglycans in Caenorhabditis elegans: embryonic cell division depends on CPG-1 and CPG-2. The Journal of Cell Biology *173*, 985-994.

Ramos-Lewis, W., and Page-McCaw, A. (2019). Basement membrane mechanics shape development: Lessons from the fly. Matrix Biol *75-76*, 72-81.

Reynolds-Peterson, C. E., Zhao, N., Xu, J., Serman, T. M., Xu, J., & Selleck, S. B. (2017). Heparan sulfate proteoglycans regulate autophagy in Drosophila. *Autophagy*, *13*(8), 1262–1279. https://doi.org/10.1080/15548627.2017.1304867

Schnorrer, F., Kalchhauser, I., & Dickson, B. J. (2007). The transmembrane protein Kon-tiki couples to Dgrip to mediate myotube targeting in Drosophila. *Developmental cell*, *12*(5), 751–766. https://doi.org/10.1016/j.devcel.2007.02.017

Spradling, A. (1993a). Developmental genetics of oogenesis. In The Development of Drosophila melanogaster (M. Bate and A. Martinez Arias, eds), pp. 1-70. Cold Spring Harbor Laboratory Press.

Suzuki, N., Toyoda, H., Sano, M., and Nishiwaki, K. (2006). Chondroitin acts in the guidance of gonadal distal tip cells in C. elegans. Dev Biol *300*, 635-646.

Takemura, M., & Nakato, H. (2017). Drosophila Sulf1 is required for the termination of intestinal stem cell division during regeneration. *Journal of cell science*, *130*(2), 332–343. https://doi.org/10.1242/jcs.195305

Takemura, M., Noborn, F., Nilsson, J., Bowden, N., Nakato, E., Baker, S., Su, T.Y., Larson, G., and Nakato, H. (2020). Chondroitin sulfate proteoglycan Windpipe modulates Hedgehog signaling in Drosophila. Mol Biol Cell *31*, 813-824.

Tian, J., Ling, L., Shboul, M., Lee, H., O'Connor, B., Merriman, B., Nelson, S.F., Cool, S., Ababneh, O.H., Al-Hadidy, A.*, et al.* (2010). Loss of CHSY1, a secreted FRINGE enzyme, causes syndromic brachydactyly in humans via increased NOTCH signaling. Am J Hum Genet *87*, 768-778.

Toyoda, H., Kinoshita-Toyoda, A., & Selleck, S. B. (2000). Structural analysis of glycosaminoglycans in Drosophila and Caenorhabditis elegans and demonstration that tout-velu, a Drosophila gene related to EXT tumor suppressors, affects heparan sulfate in vivo. *The Journal of biological chemistry*, *275*(4), 2269–2275. https://doi.org/10.1074/jbc.275.4.2269

Van De Bor, V., Loreau, V., Malbouyres, M., Cerezo, D., Placenti, A., Ruggiero, F., & Noselli, S. (2021). A dynamic and mosaic basement membrane controls cell intercalation in *Drosophila* ovaries. *Development (Cambridge, England)*, *148*(4), dev195511. https://doi.org/10.1242/dev.195511

Varki A, Cummings R, Esko J, et al., editors. Essentials of Glycobiology. Cold Spring Harbor (NY): Cold Spring Harbor Laboratory Press; 1999. Chapter 11, Proteoglycans and Glycosaminoglycans. Available from: https://www.ncbi.nlm.nih.gov/books/NBK20693/

Wang, Y., & Riechmann, V. (2007). The role of the actomyosin cytoskeleton in coordination of tissue growth during Drosophila oogenesis. *Current biology : CB*, *17*(15), 1349–1355. https://doi.org/10.1016/j.cub.2007.06.067

Wilson, D.G., Phamluong, K., Lin, W.Y., Barck, K., Carano, R.A., Diehl, L., Peterson, A.S., Martin, F., and Solloway, M.J. (2012). Chondroitin sulfate synthase 1 (Chsy1) is required for bone development and digit patterning. Dev Biol *363*, 413-425.

Xu, D., & Esko, J. D. (2014). Demystifying heparan sulfate-protein interactions. *Annual review of biochemistry*, *83*, 129–157. https://doi.org/10.1146/annurev-biochem-060713-035314

Yasothornsrikul, S., Davis, W. J., Cramer, G., Kimbrell, D. A., & Dearolf, C. R. (1997). viking: identification and characterization of a second type IV collagen in Drosophila. *Gene*, *198*(1-2), 17–25. https://doi.org/10.1016/s0378-1119(97)00274-6

Yurchenco, P. D. (2011). Basement membranes: cell scaffoldings and signaling platforms. Cold Spring Harb. Perspect. Biol. 3, 1-27. doi:10.1101/cshperspect.a004911